Contributions of Surface Solar Radiation and Precipitation to the Spatiotemporal Patterns of Surface and Air Warming in China from 1960 to 2003

Jizeng Du[1], Kaicun Wang[1*], Jiankai Wang[2], Qian Ma[1]

[1]College of Global Change and Earth System Science, Beijing Normal University, Beijing, 100875, China

[2]Chinese Meteorological Administration, Beijing, 100081, China

Corresponding author: Kaicun Wang, College of Global Change and Earth System Science, Beijing Normal University. Email: kcwang@bnu.edu.cn; Tel: +086 10-58803143; Fax: +086 10-58800059.

Submitted to Atmospheric Chemistry and Physics

March 17, 2017

Abstract

Although global warming has been attributed to increases in atmospheric greenhouses gases, the mechanisms underlying spatiotemporal patterns of warming trends remain under debate. Herein, we analyzed surface and air warming observations recorded at 1,977 stations in China from 1960 to 2003. Our results showed a significant spatial pattern for the warming of the daily maximum surface ($T_{s\text{-}max}$) and air ($T_{a\text{-}max}$) temperatures, and the pattern was stronger in northwest and northeast China and weaker or negative in South China and the North China Plain. These warming spatial patterns were attributed to surface shortwave solar radiation (R_s) and precipitation (P), which play a key role in the surface energy budget. During the study period, R_s decreased by −1.50±0.42 W m^{-2} 10yr^{-1} in China, which reduced the trends of $T_{s\text{-}max}$ and $T_{a\text{-}max}$ by about 0.139 and 0.053 °C 10yr^{-1}, respectively. More importantly, the decreasing rates in South China and the North China Plain were stronger than those in other parts of China. The spatial contrasts in the trends of $T_{s\text{-}max}$ and $T_{a\text{-}max}$ in China were significantly reduced after adjusting for the effect of R_s *and* P. For example, after adjusting for the effect of R_s *and* P, the difference in the $T_{s\text{-}max}$ and $T_{a\text{-}max}$ values between the North China Plain and the Loess Plateau was reduced by 97.8% and 68.3%, respectively, the seasonal contrast in $T_{s\text{-}max}$ and $T_{a\text{-}max}$ decreased by 45.0% and 17.2%, respectively, and the daily contrast in the warming rates of the surface and air temperature decreased by

33.0% and 29.1%, respectively. This study show that the land energy budget plays an essential role in the identification of regional warming patterns.

1. Introduction

Increases in observational data and rapid developments in simulation capacity of climate models have provided evidence for the phenomenon of global warming (Hartmann et al., 2013), and the increases in anthropogenic greenhouse gases and other anthropogenic effects are considered as the primary causes. However, significant spatial and temporal heterogeneities in climate warming have been observed. For example, faster warming rates occur in semiarid regions and a “warming hole” has been identified in the central United States (Boyles and Raman, 2003; Huang et al., 2012). These spatiotemporal heterogeneities represent a major barrier to the reliable detection and attribution of global warming (Tebaldi et al., 2005; Mahlstein and Knutti, 2010). Furthermore, uncertainties in model simulations generally increase from global to regional scales because of uncertainty in regional climatic responses to global change (Hingray et al., 2007; Mariotti et al., 2011). Therefore, investigations of the spatial and temporal patterns of regional climate changes and regional climatic response mechanisms to global change are crucial for increasing the accuracy of models designed to detect and explain the causes of global climate change and predictions of future regional climate change.

The spatial heterogeneity of climate warming can be attributed to local climate factors and anthropogenic factors (Karl et al., 1991). For the local climate factors, determining factors such as cloud cover and precipitation (*P*) can significantly influence the speed of regional warming (Hegerl and Zwiers, 2007; Lauritsen and Rogers, 2012). Spatial heterogeneities in climate-factor trends have an important influence on various changes in the land-surface energy balance. Studies have demonstrated that an increase in cloud cover can diminishes the surface solar radiation (R_s) and therefore reduces the daytime temperature (Dai et al., 1997; Zhou et al., 2010; Taylor et al., 2011), although it has the potential to increase night-time temperature by intercepting outgoing longwave radiation (Campbell and VonderHaar, 1997; Shen et al., 2014).

Precipitation (*P*) can alter the proportion of surface absorbed energy partitioned into sensible heat flux and latent heat flux; therefore it has an inevitable effect on both land-surface and near-surface air temperatures (Wang and Dickinson, 2012; Wang and Zhou, 2015). Additionally, *P* has a significant effect on soil thermal inertia and the response of surface vegetation, which results in an important feedback for regional and global warming (Seneviratne et al., 2010; Wang and Dickinson, 2012; Ait-Mesbah et al., 2015; Shen et al., 2015).

In addition to local climate factors, regional climate systems are significantly affected by the anthropogenic emissions of aerosols. Studies have indicated that improvements in air quality in recent decades over North America and Europe have led to brightening effect (Vautard et al., 2009; Wild, 2012), whereas East Asia and India have led to declines in R_s (Xia, 2010; Menon et al., 2002; Wang et al., 2012; Wang et al., 2015). Consequently, variations in R_s may have an effect on both local and global climate change (Wild et al., 2007; Wang and Dickinson, 2013a).

Changes in land cover can also alter the energy exchange between the land surface and the atmosphere, and such changes have the potential to affect regional climates (Bounoua et al., 1999; Zhou et al., 2004; Falge et al., 2005). Previous studies have suggested that urbanization and other land-use changes contribute to promoting the warming effect caused by greenhouse gases (Kalnay and Cai, 2003; Lim et al., 2005; Chen et al., 2015). Overall, the effects of these factors on climate change may be very important at the regional scale and could lead to marked spatial differences in regional climate change; however, they are usually omitted from the detection and attribution of climate change at the global scale (Karoly and Stott, 2006).

China is a vast territory that has an abundance of climactic zones stretching from tropical to cold temperate, and a special alpine climate is observed over the Tibet Plateau. Additionally, the dramatic economic development and explosive population growth in China in recent decades have caused significant changes in land cover and severe air pollution, including frequent haze events (Yin et al., 2017; Cheng et al., 2014; Wang et al., 2016). The climatic diversity and intensive human activity in this region will likely lead to a unique response to global warming with obvious spatial differences in climate change.

Karl et al. (1991) analyzed the observational records for the period 1951-1989 and found that warming trends in China were faster than those of the United States but slower than those of the former Soviet Union. Several studies have revealed that the warming rate in Northwest China was approximately 0.33-0.39 °C $10yr^{-1}$ during the second half of the last century (Zhang et al., 2010; Li et al., 2012), which was significantly higher than the average warming rate over China of 0.25 °C $10yr^{-1}$ (Ren et al., 2005) or the average global rate of 0.13 °C $10yr^{-1}$ (Hegerl and Zwiers, 2007). The air temperature (T_a) over the Tibet Plateau has increased by 0.44 °C $10yr^{-1}$ over the last 30 years (Duan and Xiao, 2015), and this rate is considerably faster than the overall warming rate in the Northern Hemisphere (0.23 °C $10yr^{-1}$) and worldwide (0.16 °C $10yr^{-1}$) (Hartmann et al., 2013). To provide insights on global warming and improve the accuracy of future climate change predictions, understanding the characteristics and mechanisms of regional climate change is critical.

T_a is a common metric for determining climate change on the global or regional scales. The land surface temperature (T_s) is also important in climate change research because of its direct relationship with the land surface energy budget. Previously, T_s values used in regional climate research are primarily derived from satellite retrievals or reanalysis datasets (Weng et al., 2004; Peng et al., 2014), which both have satisfactory global coverage but questionable accuracy and integrity. Furthermore, satellite-derived T_s values are only available under clear sky conditions, thus limiting their applicability in climate change studies.

In China, both T_s and T_a are measured as conventional meteorological observation parameters by nearly all weather stations. An analysis of the spatiotemporal patterns of these parameters identified a close relationship between T_s and T_a, which indicates that T_s and T_a present equivalent accuracy when used to determine the characteristics of climate change. More importantly, T_s is more sensitive than T_a to the local land surface energy budget.

It is well known that the diurnal cycles in T_a and T_s are primarily determined by the surface energy budget. After sunrise, the surface absorbs solar radiation, and the surface net radiation becomes positive and heats the surface first. As a result, the air above the surface becomes unstable. Surface net radiation can be partitioned into three parts: ground heat flux, sensible heat flux, and latent heat flux. Ground heat flux heats the surface and stores energy during the daytime, and this energy may be re-emitted at night. Sensible heat flux directly heats the air above the surface. Latent heat flux is the energy employed to vaporize water during the surface water evaporation and vegetation transpiration processes. How surface net radiation partitions into ground heat flux, sensible heat flux, and latent heat flux is determined by both surface and atmospheric conditions (Wang et al., 2010a; Wang et al., 2010b; Wang and Dickinson, 2012), i.e., surface wetness. Daytime surface net radiation is primarily determined by R_s (Wang and Liang, 2008) and precipitation or surface wetness control partition of surface net radiation into latent and sensible fluxes (Wang and Liang, 2008). Therefore, it is expected that changes in R_s and P play a key role in the variability of T_s and T_a (Hartmann et al., 1986; Wild, 2012; Manara et al., 2015).

However, quantitative assessments of the impact of R_s on T_s and T_a are still lack due the shortness of high quality of long-term estimates of R_s. In this study, we used sunshine duration derived R_s (Wang, 2014; Wang et al., 2015) to quantitate the impact of R_s on the spatial pattern of T_a and T_s. To our knowledge, this study presents the first analysis of the relationship between R_s (and P) and T_a (and T_s) based on their spatiotemporal patterns and we further quantified the effect of variations of R_s (and P) on T_a (and T_s) in China for the period 1960-2003.

This article is organized as follows. Section 2 introduces the data and methods used in the study. Section 3 describes the spatial and temporal patterns of climate warming over China, analyses the effect of the variation in R_s and P on T_a and T_s, and examines the spatial and temporal patterns of the warming trend of T_a and T_s after adjusting for the effects of R_s and P, which eliminated the effects of R_s and P on warming and highlighted the effects of large-scale warming caused by elevated concentrations of atmospheric greenhouse gases. Moreover, the spatial contrast in the warming trends of T_a and T_s in China was substantially reduced after adjusting for the effect of R_s and P, and this result is consistent with the expectations under global warming. Finally, Section 4 presents a summary and discussion.

2. Data and methods

2.1. Data

The meteorological observational data used in this study are included recently released daily meteorological datasets, such as the China National Stations' Fundamental Elements Datasets V3.0 (CNSFED V3.0), and they were downloaded from China's National Meteorological Information Centre (http://data.cma.gov.cn/data) (Cao et al., 2016). These datasets included observations of T_s, T_a, barometric pressure, relative humidity, and sunshine duration. All of the observational records of the climate variables were subjected to quality control measures, and the data acquisition and compilation.

As shown in Fig. 1, the number of stations used in this study (1,977 stations selected from a total of 2,479 stations) was significantly higher than that of previous studies (i.e., 57-852 stations) (Kukla and Karl, 1993; Shen and Varis, 2001; Liu et al., 2004; Li et al., 2015). Therefore, the observational data provided better spatial coverage and higher confidence in the detection of regional climate change than in previous studies (Fig. 1).

Observations of T_s from weather stations are different from T_s data retrieved via other approaches, such as satellite images and reanalysis. The T_s observations were performed in 4 × 2 m square bare land plots proximal to the weather stations. The surface of the observational fields was loose, grassless and flat, and at the same level as the ground surface of the weather station. Three thermometers, including a surface thermometer, a surface maximum thermometer, and a surface minimum thermometer were placed horizontal to the surface of the observational field, with half of each thermometer embedded in the soil and the other half exposed to the air. When the observational field was covered by snow, the thermometers were placed on the snow surface. Additionally, the exposed parts of the thermometers were cleaned to remove dust and dew.

We verified the reliability of the T_s observational records by analyzing the relationship between T_a and T_s during 1960-2003. As shown in Fig. S1, the mean Pearson correlation coefficients between daily maximum land surface temperature ($T_{s\text{-}max}$) and daily maximum air temperature ($T_{a\text{-}max}$) calculated from the monthly anomalies were 0.775, 0.843, and 0.806 for the annual, warm, and cold seasonal scales, respectively, and these values were statistically significant (99% confidence level) for all stations. The mean correlation coefficients between the daily minimum land surface temperature ($T_{s\text{-}min}$) and daily minimum air temperature ($T_{a\text{-}min}$) were 0.861, 0.842, and 0.865 for the annual, warm, and cold seasonal scales, respectively, and these values were statistically significant (99% confidence level) for all stations. The high correlations indicated that observations of either T_s or T_a could be used for climate change detection.

The most fundamental energy resource for T_s and T_a is R_s. In most previous studies, the observed R_s have been used to analyze the relation between the variation in R_s and T_a over China. However, fewer sites were used for R_s observations than for other climatic variables; for example, only 85 sites were used for R_s observations in Liu et al. (2004) and only 90 sites were used in Li et al. (2015).

Importantly, sensitivity drift the instruments used for the R_s observations led to a faster dimming rate before 1990, and instrument replacements from 1990 to 1993 resulted in a false sharp increase in R_s (Wang, 2014; Wang et al., 2015). The limited distribution and low quality of R_s observations have impeded the wide scientific application of this parameter.

Therefore, we used sunshine duration-derived R_s, which is based on an effective hybrid model developed by Yang et al. (2006). This model has subsequently been improved (Wang, 2014; Vose et al., 2005) and it has performed well in regional and global applications (Tang et al., 2011; Wang et al., 2012). Sunshine duration-derived R_s not only accurately reflects the effects of clouds and aerosols on the R_s but also more exactly reveals long-term trends (Wang, 2014; Wang et al., 2015). Additionally, sunshine duration-derived R_s values are better correlated with the satellite retrievals, reanalysis, and climate model simulations than R_s values observed from observation (Wang et al., 2015).

The data are collected by a total of 2,474 meteorological stations; however, the lengths of the effective observation records for the stations are different. Additionally, only a small number of stations were installed before 1960, and the observational records of T_s at many stations were anomalous after 2003 because of automation.

Therefore, in our analysis, we selected 1,977 meteorological stations (see Fig. 1) for which the observation records with valid data were longer than 30 years during the 43 years between 1960 and 2003.

The monthly anomalies relative to the 1961-1990 climatology were calculated based on a monthly mean value of the daily values, and when a month was missing more than 7 daily values, that month was classified as a missing value (Li et al., 2015; Sun et al., 2016). For the annual anomalies, the monthly anomalies were averaged for the entire year. The anomalies in the warm seasons were the averages of the monthly anomalies from May to October, and the anomalies in the cold seasons were the averages of the monthly anomalies from November to the next April.

2.2 Methods

As shown in Fig. 1, the spatial distribution of the weather stations throughout China is extraordinarily asymmetric and the density of weather stations in east China is far greater than that in west China. We used the area-weight average method to reduce these biases when calculating the national mean. First, we divided the study region into 1° × 1° grids (see Fig. S2) for a total 953 grids covering China. Second, we assigned all selected stations to the grids, and this resulted in 627 grids containing stations, which accounted for 65.79% of the total. Finally, the grid box value was the average of all stations in the grid, and the national mean was the area-weight average of all effective grids (Jones and Moberg, 2003).

The linear trends reported in this study were calculated via linear regression based on the monthly anomalies of T, R_s, and P. Two national mean trends were calculated from the anomalies of the grids. In the first method (Method I), the national mean monthly anomalies were calculated using the area-weight of each grid first, and then the national mean trend based on the time series of the national average anomalies was calculated. In the second method (Method II), the trend at each grid was calculated first, and then the national mean trend was calculated from the grid trends.

In our study, we calculated the national mean trends of the temperatures using Method I and II because both methods have been used in previous studies (Gettelman and Fu, 2008). The results for the two methods are expected to be the same when the time series of all grids is integrated and data are not missing (Zhou et al., 2009); however, when data are missing, small differences may occur (See Table 1). As shown in Table 1, the absolute value of the difference between Method I and Method II ranged from 0.011 to 0.033 °C $10yr^{-1}$, which represented 3.4% to 14.3% of the trends (using the results of Method I as the reference). For purposes of clarification, the trends derived from Method I are discussed in the main text, whereas the results from both methods are shown in Table 1.

The effect of R_s and P on $T_{s\text{-}max}$ and $T_{a\text{-}max}$ was determined via a multiple linear regression (Roy and Haigh, 2011) of the monthly anomalies using the following equation:

$$T = S_{R_s} \cdot R_s + S_P \cdot P + c + \varepsilon \qquad (1)$$

where T represents the monthly anomalies of $T_{s\text{-}max}$, $T_{s\text{-}min}$, $T_{a\text{-}max}$, and $T_{a\text{-}min}$; R_s and P represents the monthly anomalies of surface solar radiation and precipitation respectively. S_{Rs} and S_P are the sensitivities of temperatures to R_s and P, respectively; $\boldsymbol{c}$ is constant term; and $\boldsymbol{\varepsilon}$ indicates the residuals of the equation, which represents the contribution from other factors such as longwave radiation flux and internal variability. The coefficients of determination (R^2) for the multilinear regression equation (Eq (1)) are shown in Fig. S3, and they indicate the portion of the variance of T that could be attributed to that of R_s and P. High coefficients of determination were obtained, which showed that the linear regression performed well, particularly for South China and the North China Plain. To separate the contributions of R_s and P, we further calculated the partial correlation coefficients between R_s and T (or P and T), which are shown in Fig. S4 and Fig. S5.

To determine the effect of R_s and P on the analyzed temperatures, we removed their effects from their original time series of $T_{s\text{-}max}$ and $T_{a\text{-}max}$ based on the multilinear relationship calculated in Eq (1). Then, we calculated the trends from both the original and adjusted time series. By comparing the derived trends of the original and adjusted time series, we quantitatively assessed the effect of R_s and P on $T_{s\text{-}max}$ and $T_{a\text{-}max}$, particularly for the spatiotemporal pattern of their trends.

3. Results

3.1. Trends of surface temperature and air temperature

3.1.1 Temporal patterns in temperature variability

The long-term changes in $T_{s\text{-}max}$ and $T_{a\text{-}max}$ and $T_{s\text{-}min}$ and $T_{a\text{-}min}$ from 1960 to 2003 are shown in Fig. 2 and Fig. 3, respectively. In addition to the annual variability (Fig. 2a and Fig. 3a), the temperature variability in both warm seasons (May-October; Fig. 2b and Fig. 3b) and cold seasons (November to the following April; Fig. 2c and Fig. 3c) were analyzed. In the annual records, all temperatures exhibited an obvious warming trend throughout China (Fig. 2a and Fig. 3a).

As shown in Table 1, the national mean warming rate from 1960 to 2003 for $T_{s\text{-}max}$ was 0.227±0.091 °C 10yr^{-1} (95% confidence level) and $T_{a\text{-}max}$ was 0.167±0.068 °C

10yr^{-1} (95% confidence level). The warming rate of $T_{a\text{-}max}$ based on the 1,977 stations examined in the current study was slightly higher than the global average (0.141 °C 10yr^{-1}) from 1950 to 2004 (Vose et al., 2005) and the rate obtained from a previous analysis (0.127 °C 10yr^{-1}) of temperatures from 1955 to 2000 based on 305 stations in China (Liu et al., 2004). Additionally, the increases in $T_{s\text{-}max}$ and $T_{a\text{-}max}$ in the cold seasons were much larger than those in the warm seasons, which is consistent with previous studies of China and other regions (Vose et al., 2005; Ren et al., 2005; Shen et al., 2014).

Similarly, the warming rates of $T_{s\text{-}min}$ and $T_{a\text{-}min}$ in the warm seasons were also clearly lower than those in the cold seasons. As shown in Fig. 3, $T_{s\text{-}min}$ increased by 0.315±0.058 °C 10yr^{-1} (95% confidence level) and $T_{a\text{-}min}$ increased by 0.356±0.057 °C 10yr^{-1} (95% confidence level) (see Fig. 3a) from 1960 to 2003. The warming trend of T_a is generally consistent with earlier studies (Liu et al., 2004; Shen et al., 2014; Li et al., 2015); however, these trends are considerably larger than the rates reported for the global average (0.204 °C 10yr^{-1}) (Vose et al., 2005). For the seasonal scales, the warming rate of $T_{s\text{-}min}$ and $T_{a\text{-}min}$ in the cold seasons was almost double that of the warm seasons from 1960 to 2003 (see Table 1).

The warming rate of $T_{s\text{-}min}$ ($T_{a\text{-}min}$) was significantly faster than that of $T_{s\text{-}max}$ ($T_{a\text{-}}$

$_{max}$) and the warming rates of all temperatures in the cold seasons were substantially greater than those in the warm seasons (Easterling et al., 1997; Liu et al., 2004; Li et al., 2015). Although previous studies have indicated that the microclimate (e.g. urban heat island) has a larger effect on minimum temperatures because of the lower and more stable boundary layer at night (Christy et al., 2009; Zhou and Ren, 2011), many investigators argue that variability in R_s is the primary reason for the daily contrast in warming rates (Makowski et al., 2009; Sanchez-Lorenzo and Wild, 2012).

3.1.2. Spatial patterns in temperature variability

As shown in Fig. 4, clear spatial heterogeneity was demonstrated in the warming rates for T_{s-max} and T_{a-max} in China from 1960 to 2003. The trends of T_{s-max} and T_{a-max} were statistically higher for the Tibet Plateau, and Northwest and Northeast China (see Fig. S6) compared with the North China Plain and South China. Cooling trends in T_{s-max} even detected for the Sichuan Basin, the Yangtze River Delta, and the Pearl River Delta. Lower rates of warming of T_{a-max} in South China and the North China Plain have also been previously reported (Liu et al., 2004; Li et al., 2015).

The warming rates of T_{s-max} and T_{a-max} in South China and the North China Plain in the warm seasons were considerably lower than those in the cold seasons, which resulted in stronger spatial heterogeneity in the warm seasons (Fig. 4b and 4h). The spatial and seasonal patterns of $T_{a\text{-}max}$ were similar, although they were not as similar as the patterns of $T_{s\text{-}max}$. The spatial contrast in the trends between $T_{s\text{-}min}$ and $T_{a\text{-}min}$ was much less than that between $T_{s\text{-}max}$ and $T_{a\text{-}max}$, although a strong dependence on latitude was observed (Fig. 4d and 4j). Related studies suggested that this dependence was strongly associated with the mode variability in large-scale circulation, such as a negative trend in the North Atlantic Oscillation during this period (Wallace et al., 2012; Ding et al., 2014).

The correlation between T_s and T_a was highly significant. Based on the time series of the national mean yearly anomalies (see Fig. 2 and Fig. 3), the correlation coefficient between $T_{s\text{-}max}$ and $T_{a\text{-}max}$ was 0.877 and between $\mathrm{T_{s\text{-}min}}$ and $\mathrm{T_{a\text{-}min}}$ was 0.976 on the annual scale. In the spatial pattern of the trends (Fig. 4), the correlation coefficient between $T_{s\text{-}max}$ and $T_{a\text{-}max}$ was 0.488 and between $T_{s\text{-}min}$ and $T_{a\text{-}min}$ was 0.638 on the annual scale. All of these correlations between T_s and T_a were significant at the 95% significance level, which indicated a close relation between T_s and T_a for both interannual fluctuations and secular trends.

The correlation between $T_{s\text{-}min}$ and $T_{a\text{-}min}$ was significantly higher than that between $T_{s\text{-}max}$ and $T_{a\text{-}max}$. $T_{s\text{-}min}$ is closely related to the land-atmosphere longwave wave radiation balance at night, which is closely associated with the atmospheric greenhouse effect (Dai et al., 1999). During the day, T_s is directly determined by the land surface energy balance, i.e., the incoming energy (including R_s) and atmospheric longwave radiation (Wang and Dickinson, 2013b), and it is partitioned into latent and sensible heat fluxes (Zhou and Wang, 2016). Although T_a is dependent on the land-atmosphere sensible heat flux, it is also affected by local and/or large-scale circulation. Thus, the changes in the land surface energy balance caused by R_s and P have different levels of effect on T_s and T_a during the day, which most likely caused the lower correlation between $T_{s\text{-}max}$ and $T_{a\text{-}max}$ than that between $T_{s\text{-}min}$ and $T_{a\text{-}min}$.

3.2. Effect of R_s and P on temperatures

3.2.1 Effect of R_s

As shown in Fig. S4, R_s is closely linked with $T_{s\text{-}max}$ and $T_{a\text{-}max}$ but not with $T_{s\text{-}min}$ and $T_{a\text{-}min}$, and the correlation between $T_{s\text{-}max}$ and R_s was higher than that between $T_{a\text{-}max}$ and R_s. For the seasonal scales, the partial correlation between $T_{s\text{-}max}$ and $T_{a\text{-}max}$ and R_s in the warm seasons was stronger than that in the cold seasons, and this correlation was stronger in South China and the North China Plain. South China has high soil moisture; therefore, the relationship between the energy used for evapotranspiration and R_s is approximately linear (Zhou et al., 2007; Wang and Dickinson, 2013a). However, northwest China presents dry soil over most of the year; thus the energy used for evapotranspiration is more dependent on P. As a result, the energy available for heating the surface and air temperatures is not as closely correlated with R_s. Therefore, the correlation coefficients between R_s and $T_{s\text{-}max}$ and $T_{a\text{-}max}$ were lower in the northwest China.

To quantify the effect of R_s on temperature, the sensitivity of the studied temperatures to changes in R_s was calculated (Eq. (1)). As shown in Fig. S7 shows, $T_{s\text{-}max}$ was the most sensitive to R_s, followed by $T_{a\text{-}max}$, and the national means for $T_{s\text{-}max}$ was 0.092±0.018 °C（W m^{-2})$^{-1}$ (95% confidence level) and $T_{a\text{-}max}$ was 0.035±0.010 °C（W m^{-2})$^{-1}$ (95% confidence level). $T_{s\text{-}min}$ and $T_{a\text{-}min}$ were not sensitive to R_s because these temperatures are primarily affected by atmospheric longwave radiation night.

Based on the above analysis, we calculated the effect of changes in R_s on the studied temperatures. From 1960 to 2003, the calculations of the monthly anomalies at 1,977 stations indicated that the national mean rate of decrease of R_s was −1.502±0.42 W m^{-2} 10yr^{-1} (95% confidence level), and the trend was significant in most regions of China (see Fig. S8). Our rate of decrease was considerably less than the global average diminishing rate (form approximately −2.3 to −5.1 W m^{-2} 10yr^{-1}) between the 1960s and the 1990s (Gilgen et al., 1998; Stanhill and Cohen, 2001; Liepert, 2002; Ohmura, 2006) and the national mean dimming rate across China (from approximately −2.9 to

−5.2 W m$^{−2}$ 10yr$^{−1}$) between the 1960s and the 2000s based on radiation station observations (Che et al., 2005; Liang and Xia, 2005; Shi et al., 2008; Wang et al., 2015).

As noted in the data section, the sensitivity drift and replacement of instruments used for the R_s observations resulted in a significant homogenization of the station observation records (Wang, 2014; Wang et al., 2015), which introduced considerable uncertainty to the trend estimations. Tang et al. (2011) used quality-controlled observational data from 72 stations and two radiation models based on 479 stations to determine that the rate in China decreased from approximately −2.1 to −2.3 W m$^{−2}$ 10yr$^{−1}$ during 1961-2000, and they also showed that R_s values have remained essentially unchanged since 2000. These findings are generally consistent with our results.

Because of the decreasing trend in R_s, the national mean warming trends of $T_{s\text{-}max}$ and $T_{a\text{-}max}$ decreased by 0.139 °C 10yr$^{−1}$ and 0.053 °C 10yr$^{−1}$, respectively. Spatially, the decreasing rate of R_s in South China and the North China Plain was significantly higher than that in other regions, particularly in the warm seasons (Fig. 5b). Therefore, the cooling effect of decreasing R_s on $T_{s\text{-}max}$ and $T_{a\text{-}max}$ was more significant in South China and the China North Plain, and it resulted in significantly lower warming rates of $T_{s\text{-}max}$ and $T_{a\text{-}max}$ in those regions than in the other regions (see Fig. 4). The spatial consistency between the decreasing R_s trend and the slowdown of $T_{s\text{-}max}$ and $T_{a\text{-}max}$

warming implied that variations in R_s were the primary reason for the spatial heterogeneity of the warming rate in T_{s-max} and T_{a-max}.

3.2.2 Effect of *P*

As shown in Fig. S5, a significant negative correlation was detected between T_{s-max} and P, and the correlation was more significant in the warm seasons than in the cold seasons. P negatively correlated with temperature because P reduces temperatures by increasing the surface evaporative cooling (Dai et al., 1997; Wang et al., 2006). The national mean sensitivities of T_{s-max} and T_{a-max} to P were −0.321±0.098 °C 10 mm^{-1} and −0.064±0.054 °C 10 mm^{-1} (95% confidence level), respectively. As shown in Fig. S9, seasonal and spatial changes in the sensitivity of T_{s-max} and T_{a-max} to P were apparent (Fig. S9a–c and Fig. S9g–i). The sensitivities of T_{s-max} and T_{a-max} were significantly higher in arid regions (dry seasons) than humid regions (rainy seasons) (Wang and Dickinson, 2013a). As expected, T_{s-min} and T_{a-min} were both less sensitive to variations in the P.

The trend in P from 1960 to 2003 over the 1,977 stations showed obvious spatial heterogeneities. A slight increasing trend in P was observed in China during this period at rate of 0.112±0.718 mm 10yr^{-1} (95% confidence level). An increasing P trend was observed in northwestern China and southeastern China, whereas a decreasing trend was observed in the North China Plain, the Sichuan Basin, and parts of northeastern China. However, the P trends were not significant in most regions (see Fig. S8). Variations in P significantly differed by season (see Fig. 6b and Fig. 6c). The seasonal and spatial variations in P are consistent with those of previous studies (Zhai et al., 2005; Wang et al., 2015).

For $T_{a\text{-}max}$ and $T_{s\text{-}max}$, the warming trend in the North China Plain, the Sichuan Basin, and parts of northeastern China was aggravated by the reduction in P, whereas the warming trend in northwestern China and in the Mongolian Plateau were slowed by increases in P (Fig. 6d). For the national average, the effect of increasing P resulted in decreases in the warming trends of $T_{s\text{-}max}$ and $T_{a\text{-}max}$ by −0.007 °C $10yr^{-1}$ and −0.002 °C $10yr^{-1}$, respectively. However, the effect of P on $T_{s\text{-}max}$ was approximately an order of magnitude less than that of R_s.

3.3. Trends of surface and air temperature after adjusting for the effect of R_s and P

Based on the above analysis of the effect of R_s and P on temperatures, we found that variations in R_s and P had little effect on $T_{s\text{-}min}$ and $T_{a\text{-}min}$. However, R_s and P had important effect on the trends of $T_{s\text{-}max}$ and $T_{a\text{-}max}$ (see Fig. S3), particularly in central and South China, where $T_{s\text{-}max}$ and $T_{a\text{-}max}$ were more closely related to R_s (see Fig. S4).

Therefore, only the effects of R_s and P on $T_{s\text{-}max}$ and $T_{a\text{-}max}$ were analyzed. After adjusting for the effect of Rs and P (Fig. 7), the warming rates of $T_{s\text{-}max}$ and $T_{a\text{-}max}$ increased by 0.146 °C $10yr^{-1}$ (64.3%) and 0.055 °C $10yr^{-1}$ (33.0%), respectively. Additionally, the increasing amplitude of warming rates in the warm seasons was significantly higher than that in the cold seasons, which resulted in a seasonal contrast in warming rates, with $T_{s\text{-}max}$ and $T_{a\text{-}max}$ decreasing by 45.0% and 17.2% respectively (see Table 1).

More importantly, after adjusting for the effect of R_s and P, the spatial coherence of the warming rates of $T_{s\text{-}max}$ and $T_{a\text{-}max}$ in South China and the North China Plain clearly improved (Fig. 8). The regional differences among the North China Plain, South China, and other regions in China significantly decreased because of the increase in warming rates in South China and the North China Plain. Additionally, the warming trends of $T_{s\text{-}max}$ and $T_{a\text{-}max}$ became more statistically significant in the North China Plain and South China (see Fig. S10).

To clearly illustrate these changes, we selected two regions in China for further investigation: R1 primarily included the North China Plain and R2 primarily included the Loess Plateau (see Fig. 9a). Although these regions share the same latitudes, the trend for R_s were substantially different (see Fig. 9b). After adjusting for the effect of

R_s and P, the annual trends for $T_{s\text{-}max}$ and $T_{a\text{-}max}$ in R1 increased by 0.304 and 0.118 °C $10yr^{-1}$, respectively, whereas those in R2 increased by only 0.025 and 0.016 °C $10yr^{-1}$, respectively. Therefore, after the adjustment, the contrasts in the warming rates of $T_{s\text{-}max}$ and $T_{a\text{-}max}$ between R1 and R2 were significantly reduced (see Fig. 9d).

After the adjustment in R1, the seasonal and diurnal contrasts in the warming rates of $T_{s\text{-}max}$ and $T_{a\text{-}max}$ significantly decreased. The contrasts in warming rates between the warm seasons and cold seasons decreased by 68.7% for $T_{s\text{-}max}$ and by 50.8% for $T_{a\text{-}max}$ after the adjustment. Additionally, the contrasts in the warming rates between $T_{s\text{-}max}$ and $T_{s\text{-}min}$ decreased by 93.4% and between $T_{a\text{-}max}$ and $T_{a\text{-}min}$ decreased by 59.6% in R1. In R2, the adjustment did not significantly change the seasonal and diurnal contrasts in temperatures. Overall, the trends for R1 and R2 became more consistent after adjusting for difference in R_s and P (see Fig. 9d).

4. Conclusions and Discussion

Although a general warming trends has been observed throughout China, the regional warming trends show significant spatial and temporal heterogeneity. In this study, we analyzed the spatial and temporal patterns of T_s and T_a from 1960 to 2003 and further analyzed and quantified the effects of R_s and P on these temperatures. The primary results of the study are as follows.

The national mean warming rates from 1960 to 2003 of $T_{s\text{-}max}$, $T_{s\text{-}min}$, $T_{a\text{-}max}$, and $T_{a\text{-}min}$ were 0.227±0.091, 0.315±0.058, 0.167±0.068, and 0.356±0.057 °C $10yr^{-1}$, respectively. The warming rates of $T_{s\text{-}max}$ and $T_{a\text{-}max}$ in South China and the North China Plain were significantly lower than those in the other regions, and the spatial heterogeneity in the warm seasons was greater than that in the cold seasons.

During the study period, the R_s value decreased by −1.502±0.042 W m^{-2} $10yr^{-1}$ (95% confidence level), and higher dimming rates were observed in South China and the North China Plain. Using a partial regression analysis, we found that R_s plays a distinctly important role in the spatial warming patterns of $T_{s\text{-}max}$ and $T_{a\text{-}max}$.

After adjusting for the effect of R_s and P, the warming rates of $T_{s\text{-}max}$ and $T_{a\text{-}max}$ in South China and the North China Plain significantly increased and the regional differences in warming rates in China clearly decreased (see Fig. 8). After the adjustments, the warming rates of $T_{s\text{-}max}$ and $T_{a\text{-}max}$ in the North China Plain increased by 0.304 and 0.118 °C $10yr^{-1}$, respectively, whereas those on Loess Plateau increased only by 0.025 and 0.016 °C $10yr^{-1}$, respectively. Therefore, the differences in warming rates of $T_{s\text{-}max}$ and $T_{a\text{-}max}$ between the North China Plain and the Loess Plateau were almost eliminated (see Fig. 9d).

After adjusting for the effect of R_s and P, the warming trend of $T_{s\text{-}max}$ increased by

0.146 °C 10yr^{-1} and that of $T_{a\text{-}max}$ increased by 0.055 °C 10yr^{-1}. In addition, the trends of $T_{s\text{-}max}$ and $T_{a\text{-}max}$ became 0.373±0.068 and 0.222±0.062 °C 10yr^{-1} respectively. Reduction in R_s resulted in decreases in the warming rates of $T_{s\text{-}max}$ and $T_{a\text{-}max}$ by 0.139 °C 10yr^{-1} and 0.053 °C 10yr^{-1}, respectively, which accounted for 95.0% and 95.8% of the total effect of R_s and P, respectively. For the seasonal contrast, the warming rates of $T_{s\text{-}max}$ and $T_{a\text{-}max}$ decreased by 45.0% and 17.2%, respectively. For the daily contrast, the warming rates of T_s and T_a decreased by 33.0% and 29.1%, respectively.

In addition to R_s and P, temperature warming rates may be affected by many other factors, such as land cover and land use changes; however those factors have not been discussed in this study because of lack of data (Liu et al., 2005; Zhang et al., 2016). After adjusting for the effect of changes in R_s and P changes, the spatial differences in the warming trends clearly decreased; however, certain regional differences remained. The warming rate of $T_{s\text{-}max}$ in the Sichuan Basin remained significantly lower than that in other regions after adjusting for these effects. Additionally, the differences in the warming rates of $T_{s\text{-}min}$ and $T_{a\text{-}min}$ between the northern and southern areas were not explained by the effects of R_s and P; further study is required.

Acknowledgements The National Natural Science Foundation of China (grant no. 41525018 and 91337111) and the National Basic Research Program of China funded this study (grant no. 2012CB955302). The land surface temperatures and sunshine duration datasets that include data from approximately 2,400 meteorological stations in China from 1960 to 2003, are obtained from the China Meteorological Administration (CMA, http://data.cma.gov.cn/data).

References

Ait-Mesbah, S., Dufresne, J. L., Cheruy, F., and Hourdin, F.: The role of thermal inertia in the representation of mean and diurnal range of surface temperature in semiarid and arid regions, Geophys Res Lett, 42, 7572-7580, 10.1002/2015gl065553, 2015.

Bounoua, L., Collatz, G. J., Sellers, P. J., Randall, D. A., Dazlich, D. A., Los, S. O., Berry, J. A., Fung, I., Tucker, C. J., Field, C. B., and Jensen, T. G.: Interactions between vegetation and climate: Radiative and physiological effects of doubled atmospheric CO2, J Climate, 12, 309-324, 10.1175/1520-0442(1999)012<0309:ibvacr>2.0.co;2, 1999.

Boyles, R. P., and Raman, S.: Analysis of climate trends in North Carolina (1949-1998), Environ Int, 29, 263-275, 10.1016/s0160-4120(02)00185-x, 2003.

Campbell, G. G., and VonderHaar, T. H.: Comparison of surface temperature minimum and maximum and satellite measured cloudiness and radiation budget, J Geophys Res-Atmos, 102, 16639-16645, 10.1029/96jd02718, 1997.

Cao, L., Zhu, Y., Tang, G., Yuan, F., and Yan, Z.: Climatic warming in China according to a homogenized data set from 2419 stations, Int J Climatol, 36, 4384-4392, 10.1002/joc.4639, 2016.

Che, H. Z., Shi, G. Y., Zhang, X. Y., Arimoto, R., Zhao, J. Q., Xu, L., Wang, B., and Chen, Z. H.: Analysis of 40 years of solar radiation data from China, 1961-2000, Geophys Res Lett, 32, L06803, 10.1029/2004gl022322, 2005.

Chen, H. S., Ma, H. D., Li, X., and Sun, S. L.: Solar influences on spatial patterns of Eurasian winter temperature and atmospheric general circulation anomalies, J Geophys Res-Atmos, 120, 8642-8657, 10.1002/2015jd023415, 2015.

Cheng, Z., Wang, S., Fu, X., Watson, J. G., Jiang, J., Fu, Q., Chen, C., Xu, B., Yu, J., Chow, J. C., and Hao, J.: Impact of biomass burning on haze pollution in the Yangtze River delta, China: a case study in summer 2011, Atmos. Chem. Phys., 14, 4573-4585, 10.5194/acp-14-4573-2014, 2014.

Christy, J. R., Norris, W. B., and McNider, R. T.: Surface Temperature Variations in East Africa and Possible Causes, J Climate, 22, 3342-3356, 10.1175/2008jcli2726.1, 2009.

Dai, A., DelGenio, A. D., and Fung, I. Y.: Clouds, precipitation and temperature range, Nature, 386, 665-666, 10.1038/386665b0, 1997.

Dai, A., Trenberth, K. E., and Karl, T. R.: Effects of clouds, soil moisture, precipitation, and water vapor on diurnal temperature range, J Climate, 12, 2451-2473, 10.1175/1520-0442(1999)012<2451:eocsmp>2.0.co;2, 1999.

Ding, Q., Wallace, J. M., Battisti, D. S., Steig, E. J., Gallant, A. J. E., Kim, H.-J., and Geng, L.: Tropical forcing of the recent rapid Arctic warming in northeastern Canada and Greenland, Nature, 509, 209-212, 10.1038/nature13260, 2014.

Duan, A., and Xiao, Z.: Does the climate warming hiatus exist over the Tibetan Plateau?, Sci. Rep, 5, 13711, 10.1038/srep13711, 2015.

Easterling, D. R., Horton, B., Jones, P. D., Peterson, T. C., Karl, T. R., Parker, D. E., Salinger, M. J., Razuvayev, V., Plummer, N., Jamason, P., and Folland, C. K.: Maximum and minimum temperature trends for the globe, Science, 277, 364-367, 10.1126/science.277.5324.364, 1997.

Falge, E., Reth, S., Bruggemann, N., Butterbach-Bahl, K., Goldberg, V., Oltchev, A., Schaaf, S., Spindler, G., Stiller, B., Queck, R., Kostner, B., and Bernhofer, C.: Comparison of surface energy exchange models with eddy flux data in forest and grassland ecosystems of Germany, Ecol Model, 188, 174-216, 10.1016/j.ecolmodel.2005.01.057, 2005.

Gettelman, A., and Fu, Q.: Observed and simulated upper-tropospheric water vapor feedback, J Climate, 21, 3282-3289, 10.1175/2007jcli2142.1, 2008.

Gilgen, H., Wild, M., and Ohmura, A.: Means and trends of shortwave irradiance at the surface estimated from global energy balance archive data, J Climate, 11, 2042-2061, 10.1175/1520-0442-11.8.2042, 1998.

Hartmann, D. L., Ramanathan, V., Berroir, A., and Hunt, G. E.: Earth radiation budget data and climate research, Rev Geophys, 24, 439-468, 10.1029/RG024i002p00439, 1986.

Hartmann, D. L., Tank, A. M. G. K., and Rusticucci, M.: Observation: Atmosphere and surface, IPCC, 161-218, 10.1017/CBO09781107415324, 2013.

Hegerl, G. C., and Zwiers, F. W.: Climate change 2007: Understanding and attributing climate change, IPCC, 665-744, 10.1017/CBO9781107415324, 2007.

Hingray, B., Mezghani, A., and Buishand, T. A.: Development of probability distributions for regional climate change from uncertain global mean warming and an uncertain scaling relationship, Hydrol Earth Syst Sc, 11, 1097-1114, 10.5194/hess-11-1097-2007, 2007.

Huang, J., Guan, X., and Ji, F.: Enhanced cold-season warming in semi-arid regions, Atmos. Chem. Phys., 12, 5391-5398, 10.5194/acp-12-5391-2012, 2012.

Jones, P. D., and Moberg, A.: Hemispheric and large-scale surface air temperature variations: An extensive revision and an update to 2001, J Climate, 16, 206-223, 10.1175/1520-0442(2003)016<0206:halssa>2.0.co;2, 2003.

Kalnay, E., and Cai, M.: Impact of urbanization and land-use change on climate, Nature, 423, 528-531, 10.1038/nature01675, 2003.

Karl, T. R., Kukla, G., Razuvayev, V. N., Changery, M. J., Quayle, R. G., Heim, R. R., Easterling, D. R., and Fu, C. B.: Global warming - evidence for asymmetric diurnal temperature-change, Geophys Res Lett, 18, 2253-2256, 10.1029/91gl02900, 1991.

Karoly, D. J., and Stott, P. A.: Anthropogenic warming of central England temperature, Atmos. Sci. Lett., 7, 81-85, 10.1002/asl.136, 2006.

Kukla, G., and Karl, T. R.: Nighttime warming and the greenhouse-effect, Environ Sci Technol, 27, 1468-1474, 10.1021/es00045a001, 1993.

Lauritsen, R. G., and Rogers, J. C.: US Diurnal Temperature Range Variability and Regional Causal Mechanisms, 1901-2002, J Climate, 25, 7216-7231, 10.1175/jcli-d-11-00429.1, 2012.

Li, B. F., Chen, Y. N., and Shi, X.: Why does the temperature rise faster in the arid region of northwest China?, J Geophys Res-Atmos, 117, D16115, 10.1029/2012jd017953, 2012.

Li, Q. X., Yang, S., Xu, W. H., Wang, X. L. L., Jones, P., Parker, D., Zhou, L. M., Feng, Y., and Gao, Y.: China experiencing the recent warming hiatus, Geophys Res Lett, 42, 889-898, 10.1002/2014gl062773, 2015.

Liang, F., and Xia, X. A.: Long-term trends in solar radiation and the associated climatic factors over China for 1961-2000, Ann Geophys, 23, 2425-2432, 10.5194/angeo-23-2425-2005, 2005.

Liepert, B. G.: Observed reductions of surface solar radiation at sites in the United States and worldwide from 1961 to 1990, Geophys Res Lett, 29, 1421, 10.1029/2002gl014910, 2002.

Lim, Y. K., Cai, M., Kalnay, E., and Zhou, L. M.: Observational evidence of sensitivity of surface climate changes to land types and urbanization, Geophys Res Lett, 32, L22712, 10.1029/2005gl024267, 2005.

Liu, B. H., Xu, M., Henderson, M., Qi, Y., and Li, Y. Q.: Taking China's temperature: Daily range, warming trends, and regional variations, 1955-2000, J Climate, 17, 4453-4462, 10.1175/3230.1, 2004.

Liu, J. Y., Liu, M. L., Tian, H. Q., Zhuang, D. F., Zhang, Z. X., Zhang, W., Tang, X. M., and Deng, X. Z.: Spatial and temporal patterns of China's cropland during 1990-2000: An analysis based on Landsat TM data, Remote Sens Environ, 98, 442-456, 10.1016/j.rse.2005.08.012, 2005.

Mahlstein, I., and Knutti, R.: Regional climate change patterns identified by cluster analysis, Clim Dynam, 35, 587-600, 10.1007/s00382-009-0654-0, 2010.

Makowski, K., Jaeger, E. B., Chiacchio, M., Wild, M., Ewen, T., and Ohmura, A.: On the relationship between diurnal temperature range and surface solar radiation in Europe, J Geophys Res-Atmos, 114, D00D07, 10.1029/2008JD011104, 2009.

Manara, V., Beltrano, M. C., Brunetti, M., Maugeri, M., Sanchez-Lorenzo, A., Simolo, C., and Sorrenti, S.: Sunshine duration variability and trends in Italy from homogenized instrumental time series (1936-2013), J Geophys Res-Atmos, 120, 3622-3641, 10.1002/2014jd022560, 2015.

Mariotti, L., Coppola, E., Sylla, M. B., Giorgi, F., and Piani, C.: Regional climate model simulation of projected 21st century climate change over an all-Africa domain: Comparison analysis of nested and driving model results, J Geophys Res-Atmos, 116, D15111, 10.1029/2010jd015068, 2011.

Menon, S., Hansen, J., Nazarenko, L., and Luo, Y. F.: Climate effects of black carbon aerosols in China and India, Science, 297, 2250-2253, 10.1126/science.1075159, 2002.

Ohmura, A.: Observed long-term variations of solar irradiance at the earth's surface, Space Sci Rev, 125, 111-128, 10.1007/s11214-006-9050-9, 2006.

Peng, S. S., Piao, S. L., Zeng, Z. Z., Ciais, P., Zhou, L. M., Li, L. Z. X., Myneni, R. B., Yin, Y., and Zeng, H.: Afforestation in China cools local land surface temperature, P Natl Acad Sci USA, 111, 2915-2919, 10.1073/pnas.1315126111, 2014.

Ren, G., Xu, M., Chu, Z., Guo, J., Li, Q., Liu, X., and Wang, Y.: Changes of Surface Air Temperature in China During 1951-2004, Climatic and environmental research, 10, 717-727, 2005.

Roy, I., and Haigh, J. D.: The influence of solar variability and the quasi-biennial oscillation on lower atmospheric temperatures and sea level pressure, Atmos. Chem. Phys., 11, 11679-11687, 10.5194/acp-11-11679-2011, 2011.

Sanchez-Lorenzo, A., and Wild, M.: Decadal variations in estimated surface solar radiation over Switzerland since the late 19th century, Atmos. Chem. Phys., 12, 8635-8644, 10.5194/acp-12-8635-2012, 2012.

Seneviratne, S. I., Corti, T., Davin, E. L., Hirschi, M., Jaeger, E. B., Lehner, I., Orlowsky, B., and Teuling, A. J.: Investigating soil moisture-climate interactions in a changing climate: A review, Earth-sci Rev, 99, 125-161, 10.1016/j.earscirev.2010.02.004, 2010.

Shen, D. J., and Varis, O.: Climate change in China, Ambio, 30, 381-383, 10.1639/0044-7447(2001)030[0381:ccic]2.0.co;2, 2001.

Shen, M. G., Piao, S. L., Jeong, S. J., Zhou, L. M., Zeng, Z. Z., Ciais, P., Chen, D. L., Huang, M. T., Jin, C. S., Li, L. Z. X., Li, Y., Myneni, R. B., Yang, K., Zhang, G. X., Zhang, Y. J., and Yao, T. D.: Evaporative cooling over the Tibetan Plateau induced by vegetation growth, P Natl Acad Sci USA, 112, 9299-9304, 10.1073/pnas.1504418112, 2015.

Shen, X. J., Liu, B. H., Li, G. D., Wu, Z. F., Jin, Y. H., Yu, P. J., and Zhou, D. W.: Spatiotemporal change of diurnal temperature range and its relationship with sunshine duration and precipitation in China, J Geophys Res-Atmos, 119, 13163-13179, 10.1002/2014jd022326, 2014.

Shi, G. Y., Hayasaka, T., Ohmura, A., Chen, Z. H., Wang, B., Zhao, J. Q., Che, H. Z., and Xu, L.: Data quality assessment and the long-term trend of ground solar radiation in China, J. Appl. Meteorol. Clim., 47, 1006-1016, 10.1175/2007jamc1493.1, 2008.

Stanhill, G., and Cohen, S.: Global dimming: a review of the evidence for a widespread and significant reduction in global radiation with discussion of its probable causes and possible agricultural consequences, Agr Forest Meteorol, 107, 255-278, 10.1016/s0168-1923(00)00241-0, 2001.

Sun, Y., Zhang, X. B., Ren, G. Y., Zwiers, F. W., and Hu, T.: Contribution of urbanization to warming in China, Nature Climate Change, 6, 706-709, 10.1038/nclimate2956, 2016.

Tang, W. J., Yang, K., Qin, J., Cheng, C. C. K., and He, J.: Solar radiation trend across China in recent decades: a revisit with quality-controlled data, Atmos. Chem. Phys., 11, 393-406, 10.5194/acp-11-393-2011, 2011.

Taylor, J. R., Randel, W. J., and Jensen, E. J.: Cirrus cloud-temperature interactions in the tropical tropopause layer: a case study, Atmos. Chem. Phys., 11, 10085-10095, 10.5194/acp-11-10085-2011, 2011.

Tebaldi, C., Smith, R. L., Nychka, D., and Mearns, L. O.: Quantifying uncertainty in projections of regional climate change: A Bayesian approach (vol 18, pg 1524, 2005), J Climate, 18, 3405-3405, 10.1175/JCLI9001.1a, 2005.

Vautard, R., Yiou, P., and van Oldenborgh, G. J.: Decline of fog, mist and haze in Europe over the past 30 years, Nat Geosci, 2, 115-119, 10.1038/ngeo414, 2009.

Vose, R. S., Easterling, D. R., and Gleason, B.: Maximum and minimum temperature trends for the globe: An update through 2004, Geophys Res Lett, 32, L23822, 10.1029/2005gl024379, 2005.

Wallace, J. M., Fu, Q., Smoliak, B. V., Lin, P., and Johanson, C. M.: Simulated versus observed patterns of warming over the extratropical Northern Hemisphere continents during the cold season, P Natl Acad Sci USA, 109, 14337-14342, 10.1073/pnas.1204875109, 2012.

Wang, K., Dickinson, R. E., Wild, M., and Liang, S.: Evidence for decadal variation in global terrestrial evapotranspiration between 1982 and 2002: 1. Model development, J Geophys Res-Atmos, 115, D20112, 10.1029/2010JD013847, 2010a.

Wang, K., Dickinson, R. E., Wild, M., and Liang, S.: Evidence for decadal variation in global terrestrial evapotranspiration between 1982 and 2002: 2. Results, J Geophys Res-Atmos, 115, D20113, 10.1029/2009JD013671, 2010b.

Wang, K., and Dickinson, R. E.: Contribution of solar radiation to decadal temperature variability over land, P Natl Acad Sci USA, 110, 14877-14882, 10.1073/pnas.1311433110, 2013a.

Wang, K., and Dickinson, R. E.: Global atmospheric downward longwave radiation at the surface from ground-based observations, satellite retrievals, and reanalyses, Rev Geophys, 51, 150-185, 10.1002/rog.20009, 2013b.

Wang, K., Ma, Q., Li, Z., and Wang, J.: Decadal variability of surface incident solar radiation over China: Observations, satellite retrievals, and reanalyses, J Geophys Res-Atmos, 120, 6500-6514, 10.1002/2015jd023420, 2015.

Wang, K. C., Li, Z. Q., and Cribb, M.: Estimation of evaporative fraction from a combination of day and night land surface temperatures and NDVI: A new method to determine the Priestley-Taylor parameter, Remote Sens Environ, 102, 293-305, 10.1016/j.rse.2006.02.007, 2006.

Wang, K. C., and Liang, S. L.: Estimation of Daytime Net Radiation from Shortwave Radiation Measurements and Meteorological Observations, J. Appl. Meteorol. Clim., 48, 634-643, 10.1175/2008jamc1959.1, 2008.

Wang, K. C., and Dickinson, R. E.: A review of global terrestrial evapotranspiration: Observation, modeling, climatology, and climatic variability, Rev Geophys, 50, RG2005, 10.1029/2011rg000373, 2012.

Wang, K. C., Dickinson, R. E., Wild, M., and Liang, S.: Atmospheric impacts on climatic variability of surface incident solar radiation, Atmos. Chem. Phys., 12, 9581-9592, 10.5194/acp-12-9581-2012, 2012.

Wang, K. C.: Measurement Biases Explain Discrepancies between the Observed and Simulated Decadal Variability of Surface Incident Solar Radiation, Sci. Rep, 4, 6144, 10.1038/srep06144, 2014.

Wang, K. C., and Zhou, C. L. E.: Regional Contrasts of the Warming Rate over Land Significantly Depend on the Calculation Methods of Mean Air Temperature, Sci. Rep, 5, 12324, 10.1038/srep12324, 2015.

Wang, X., Wang, K., and Su, L.: Contribution of Atmospheric Diffusion Conditions to the Recent Improvement in Air Quality in China, Sci. Rep, 6, 36404, 10.1038/srep36404, 2016.

Weng, Q. H., Lu, D. S., and Schubring, J.: Estimation of land surface temperature-vegetation abundance relationship for urban heat island studies, Remote Sens Environ, 89, 467-483, 10.1016/j.rse.2003.11.005, 2004.

Wild, M., Ohmura, A., and Makowski, K.: Impact of global dimming and brightening on global warming, Geophys Res Lett, 34, L04702, 10.1029/2006gl028031, 2007.

Wild, M.: Enlightening global dimming and brightening, B Am Meteorol Soc, 93, 27-37, 10.1175/bams-d-11-00074.1, 2012.

Xia, X.: A closer looking at dimming and brightening in China during 1961-2005, Ann Geophys, 28, 1121-1132, 10.5194/angeo-28-1121-2010, 2010.

Yang, K., Koike, T., and Ye, B. S.: Improving estimation of hourly, daily, and monthly solar radiation by importing global data sets, Agr Forest Meteorol, 137, 43-55, 10.1016/j.agrformet.2006.02.001, 2006.

Yin, Z., Wang, H., and Chen, H.: Understanding Severe Winter Haze Pollution in the North-Central North China Plain in 2014, Atmos. Chem. Phys., 17, 1641-1651, 10.5194/acp-2016-641, 2017.

You, Q. L., Min, J. Z., Jiao, Y., Sillanpaa, M., and Kang, S. C.: Observed trend of diurnal temperature range in the Tibetan Plateau in recent decades, Int J Climatol, 36, 2633-2643, 10.1002/joc.4517, 2016.

Zhai, P. M., Zhang, X. B., Wan, H., and Pan, X. H.: Trends in total precipitation and frequency of daily precipitation extremes over China, J Climate, 18, 1096-1108, 10.1175/jcli-3318.1, 2005.

Zhang, X., Sun, Y., Mao, W., Liu, Y., and Ren, Y.: Regional Response of Temperature Change in the Arid Regions of China to Global Warming, Arid Zone Research, 27, 592-599, 2010.

Zhang, Z. X., Li, N., Wang, X., Liu, F., and Yang, L. P.: A Comparative Study of Urban Expansion in Beijing, Tianjin and Tangshan from the 1970s to 2013, Remote. Sen., 8, 496, 10.3390/rs8060496, 2016.

Zhou, C. L., and Wang, K. C.: Coldest Temperature Extreme Monotonically Increased and Hottest Extreme Oscillated over Northern Hemisphere Land during Last 114 Years, Sci. Rep, 6, 25721, 10.1038/srep25721, 2016.

Zhou, L. M., Dickinson, R. E., Tian, Y. H., Fang, J. Y., Li, Q. X., Kaufmann, R. K., Tucker, C. J., and Myneni, R. B.: Evidence for a significant urbanization effect on climate in China, P Natl Acad Sci USA, 101, 9540-9544, 10.1073/pnas.0400357101, 2004.

Zhou, L. M., Dickinson, R. E., Tian, Y. H., Vose, R. S., and Dai, Y. J.: Impact of vegetation removal and soil aridation on diurnal temperature range in a semiarid region: Application to the Sahel, P Natl Acad Sci USA, 104, 17937-17942, 10.1073/pnas.0700290104, 2007.

Zhou, L. M., Dai, A., Dai, Y. J., Vose, R., Zou, C. Z., Tian, Y. H., and Chen, H. S.: Spatial dependence of diurnal temperature range trends on precipitation from 1950 to 2004, Clim Dynam, 32, 429-440, 10.1007/s00382-008-0387-5, 2009.

Zhou, L. M., Dickinson, R. E., Dai, A. G., and Dirmeyer, P.: Detection and attribution of anthropogenic forcing to diurnal temperature range changes from 1950 to 1999: comparing multi-model simulations with observations, Clim Dynam, 35, 1289-1307, 10.1007/s00382-009-0644-2, 2010.

Zhou, Y. Q., and Ren, G. Y.: Change in extreme temperature event frequency over mainland China, 1961-2008, Climate Res, 50, 125-139, 10.3354/cr01053, 2011.

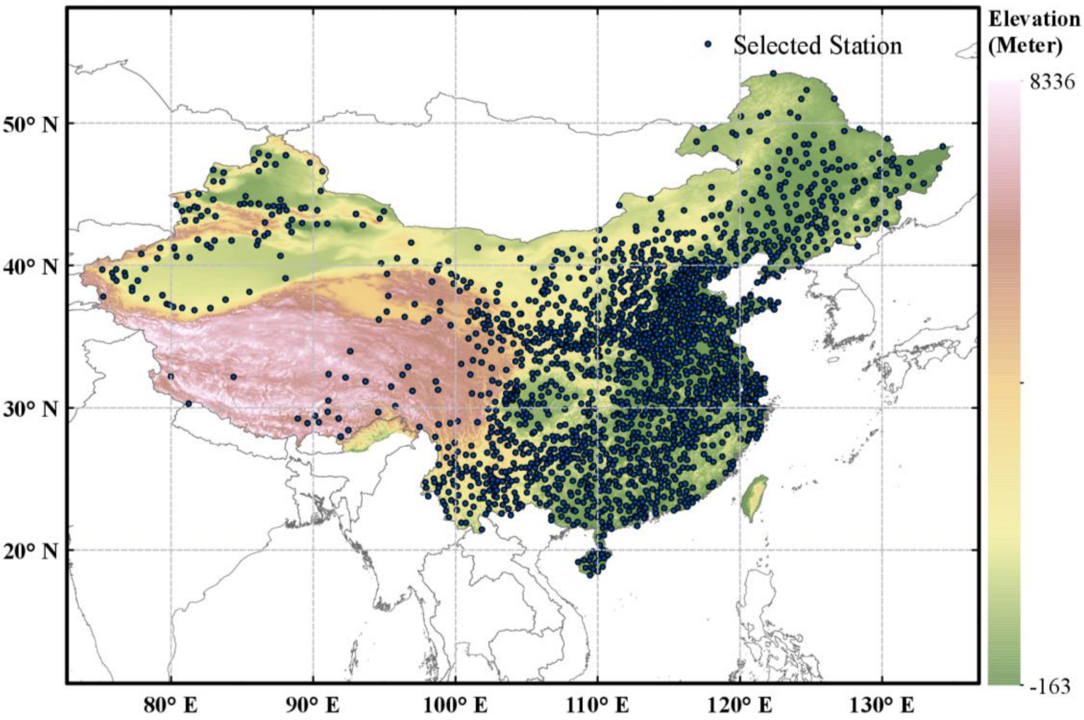

Figure 1. Elevation maps of mainland China and spatial distribution of the 1977 meteorological stations used in this study. The datasets were provided by China’s National Meteorological Information Centre (You et al., 2016) (**http://data.cma.gov.cn/data**).

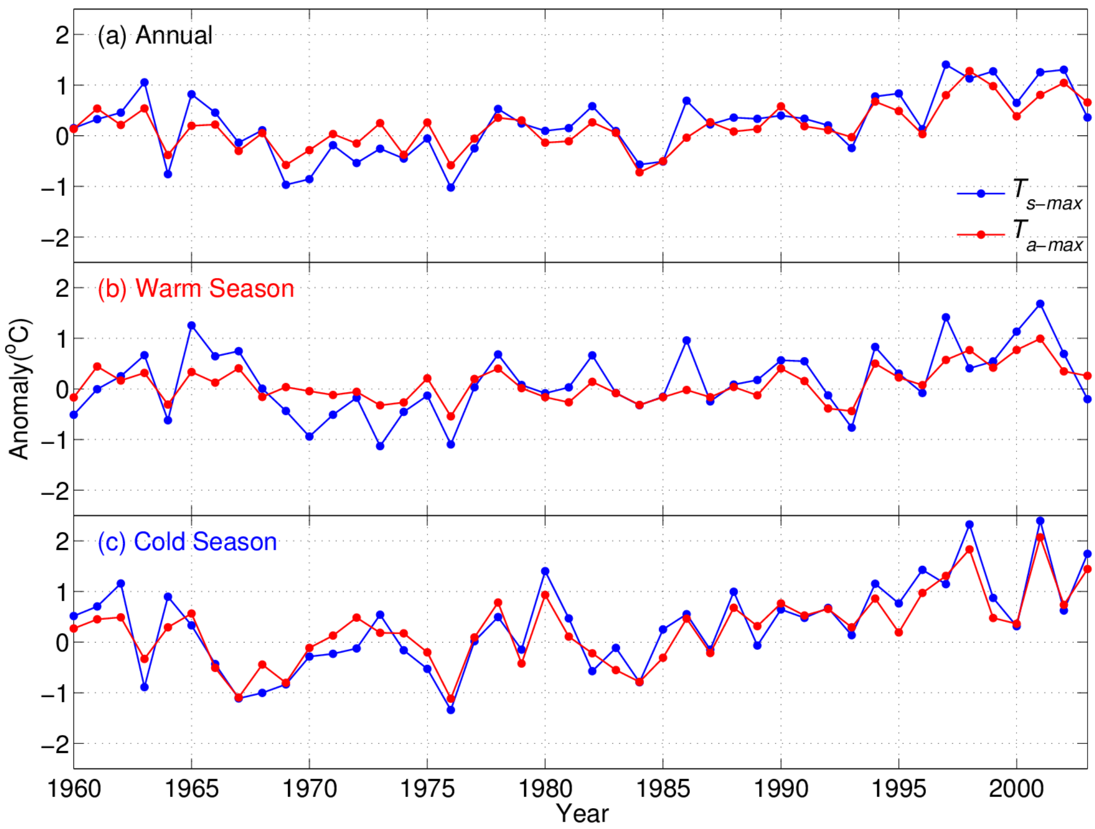

Figure 2. National mean yearly anomalies of daily maximum land surface temperature ($T_{s\text{-}max}$, blue line) and daily maximum air temperature ($T_{a\text{-}max}$, red line) for the annual (a), warm (b), and cold (c) seasonal scales for the reference period from 1961 to 1990.

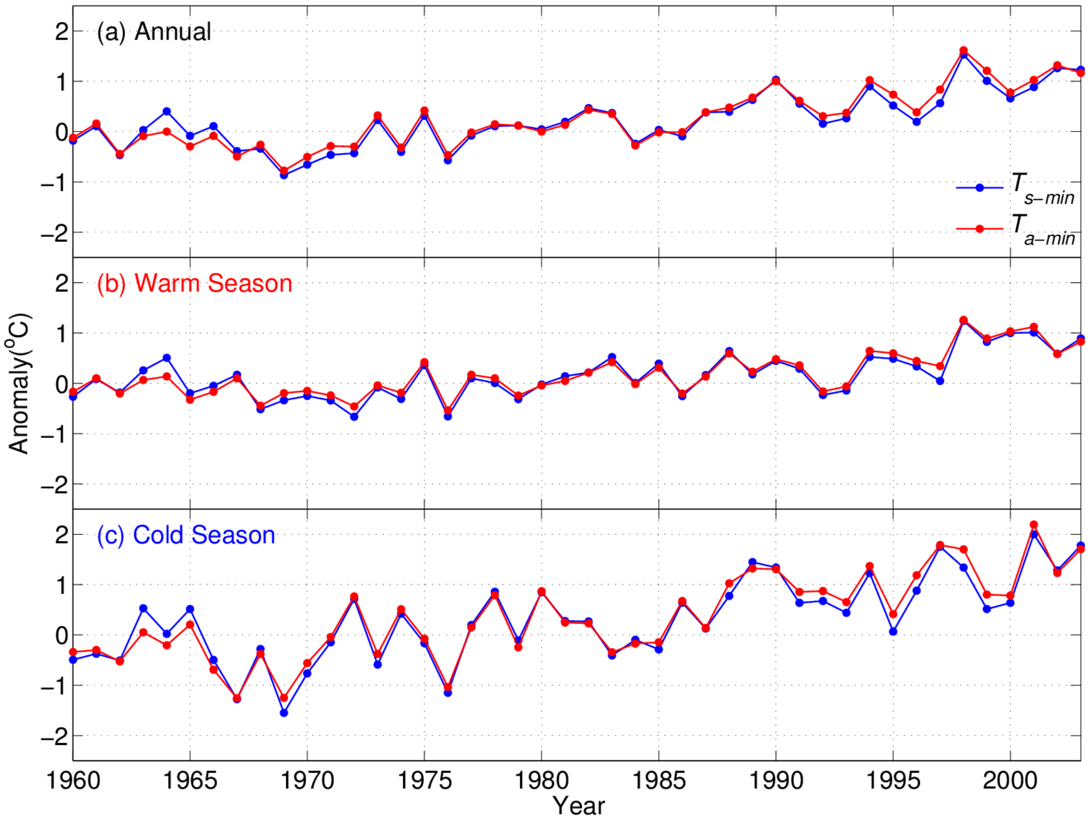

Figure 3. National mean yearly anomalies of daily minimum land surface temperature ($T_{s\text{-}min}$, blue line) and daily minimum air temperature ($T_{a\text{-}min}$, red line) for the annual (a), warm (b), and cold (c) seasonal scales for the reference period 1961-1990.

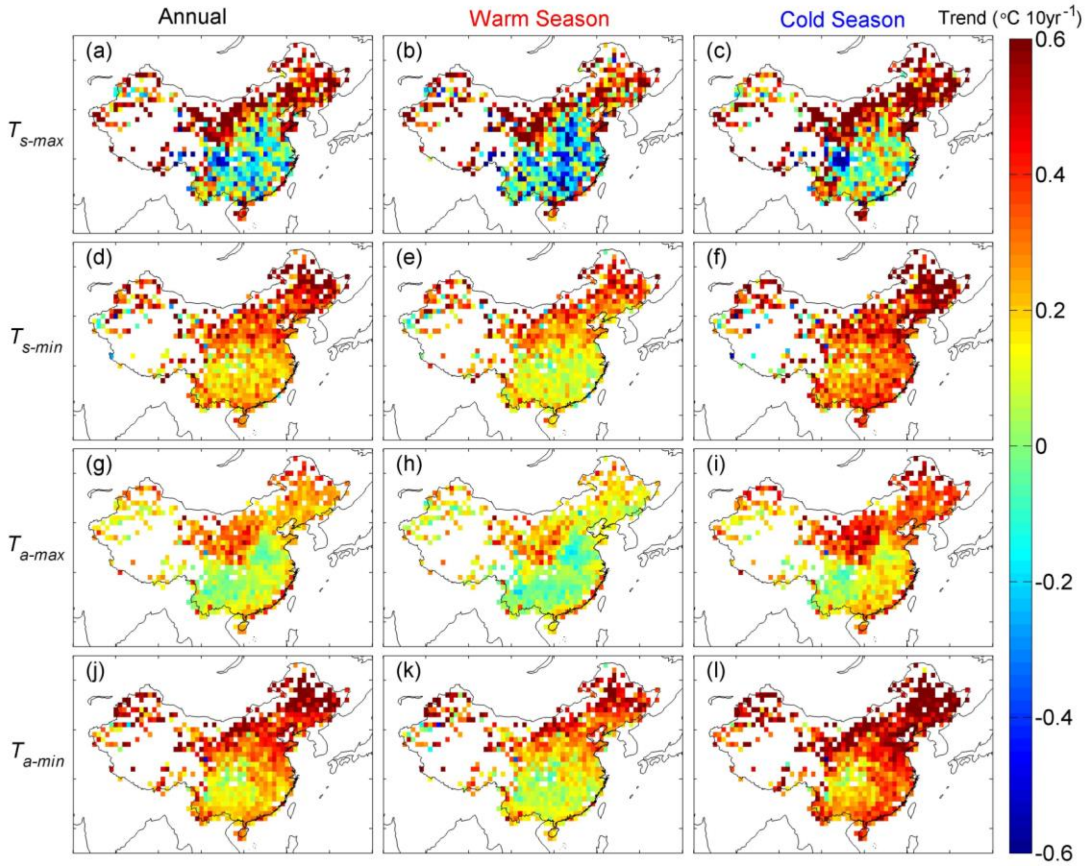

Figure 4. Maps of the trends of the monthly anomalies for daily maximum land surface temperature (T_{s-max}, a-c), daily minimum land surface temperature (T_{s-min}, d-f), daily maximum air temperature (T_{a-max}, g-i), and daily minimum air temperature (T_{a-min}, j-l) for the annual, warm (May-October), and cold (November-next April) seasonal scales. All trends reported in these figures were calculated using a linear regression based on the least square method.

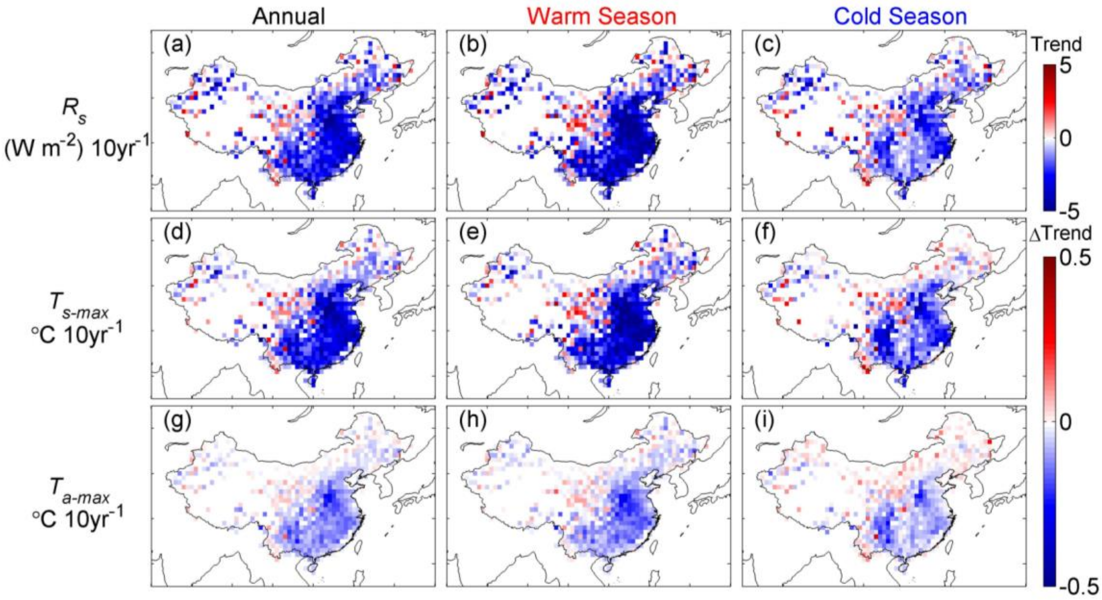

Figure 5. Maps of the trends in surface solar radiation (R_s, a-c) and its effect on the warming rates of daily maximum land surface temperature ($T_{s\text{-}max}$, d-f) and daily maximum air temperature ($T_{a\text{-}max}$, g-i). The first line (a-c) is the trend of R_s from 1960-2003; the second line (d-f) and the third line (g-i) are the trend changes caused by secular variations of R_s on $T_{s\text{-}max}$ and $T_{a\text{-}max}$. Eq (1) was used to strip away the effect of R_s on temperatures, and we calculated the trend difference (ΔTrend, d-i) between the time series of temperatures before and after adjusting for the effect of R_s. Finally, the effect of R_s on the trends of $T_{s\text{-}max}$ and $T_{a\text{-}max}$ was quantified and analyzed (section 3.2.1).

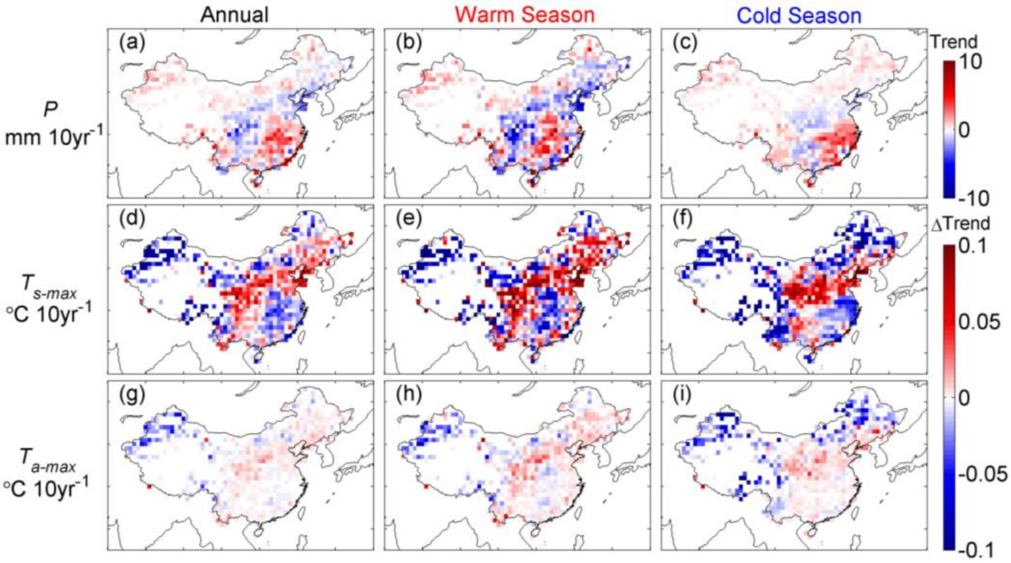

Figure 6. Maps of the trends in precipitation (*P*) (a-c) and their effect on the warming rates for daily maximum land surface temperature ($T_{s\text{-}max}$, d-f) and daily maximum air temperature ($T_{a\text{-}max}$, g-i). The first line (a-c) is the trend of *P* during 1960-2003; the second line (d-f) and the third line (g-i) are the trend changes caused by secular variations of *P* on $T_{s\text{-}max}$ and $T_{a\text{-}max}$. We used Eq (1) to remove the effects of *P* on the temperatures, then calculated the trend difference (ΔTrend, d-i) between the time series of temperatures before and after adjusting for the effect of *P*. Finally, the effect of *P* on the trends of $T_{s\text{-}max}$ and $T_{a\text{-}max}$ was quantified and analyzed (section 3.2.2).

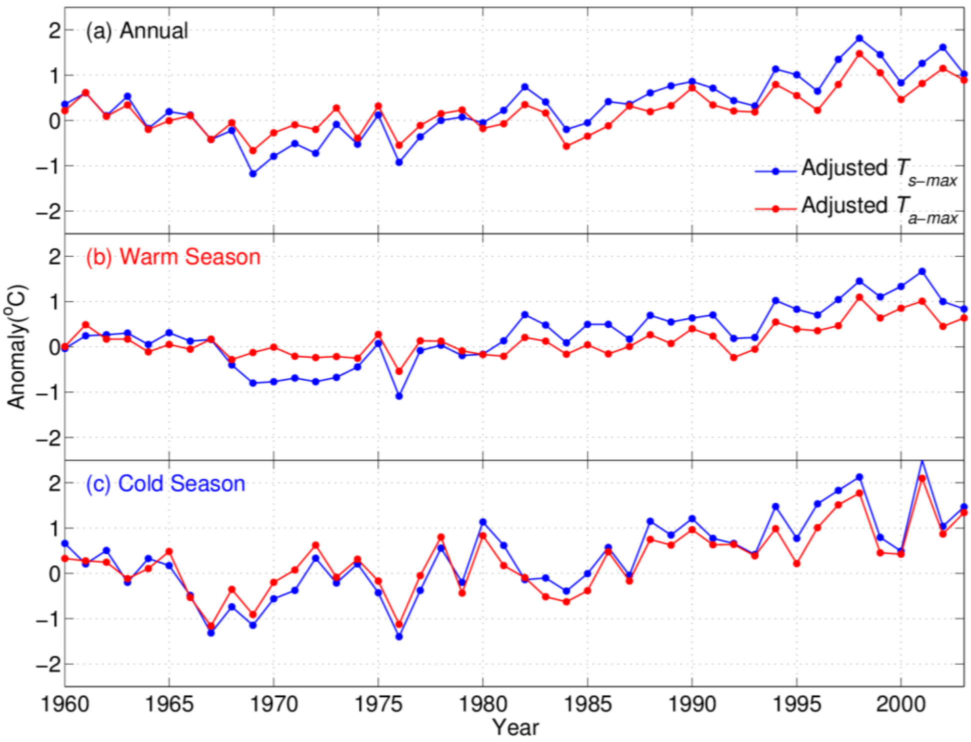

Figure 7. Regional average anomalies of daily maximum land surface temperature (T_{s-max}, blue line) and daily maximum air temperature (T_{a-max}, red line) for the annual (a), warm (b), and cold (c) seasonal scales for the reference period from 1961 to 1990. We used Eq (1) to simultaneously adjust for the effects of surface solar radiation (R_s) and precipitation (P) on T_{s-max} and T_{a-max} and then analyzed the changes in the interannual variation of T_{s-max} and T_{a-max} (section 3.3).

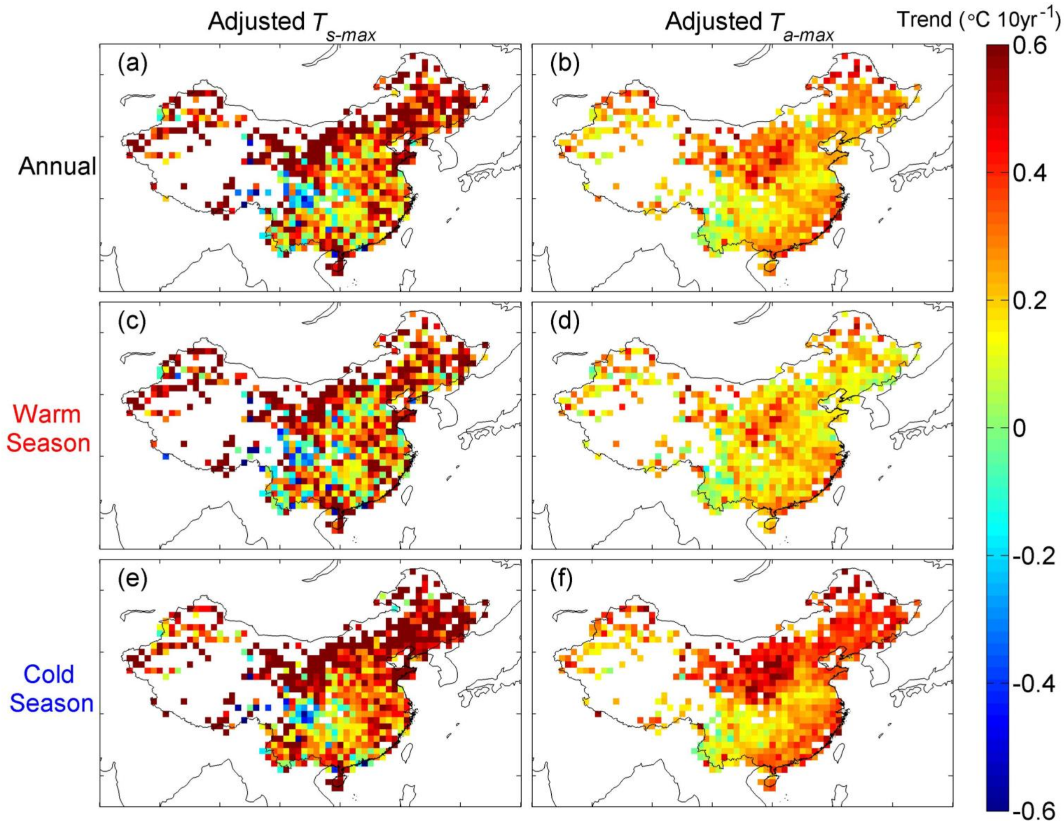

Figure 8. Maps of the trends of the monthly anomalies for the daily maximum land surface temperature ($T_{s\text{-}max}$, a, c, e) and daily maximum air temperature ($T_{a\text{-}max}$, b, d, f) for the annual, warm, and cold seasonal scales after adjusting for the effects of surface solar radiation (R_s) and precipitation (P). We used Eq (1) to simultaneously adjust the effects of R_s and P on $T_{s\text{-}max}$ and $T_{a\text{-}max}$ and then analyzed the changes in the secular trends of $T_{s\text{-}max}$ and $T_{a\text{-}max}$ (section 3.3).

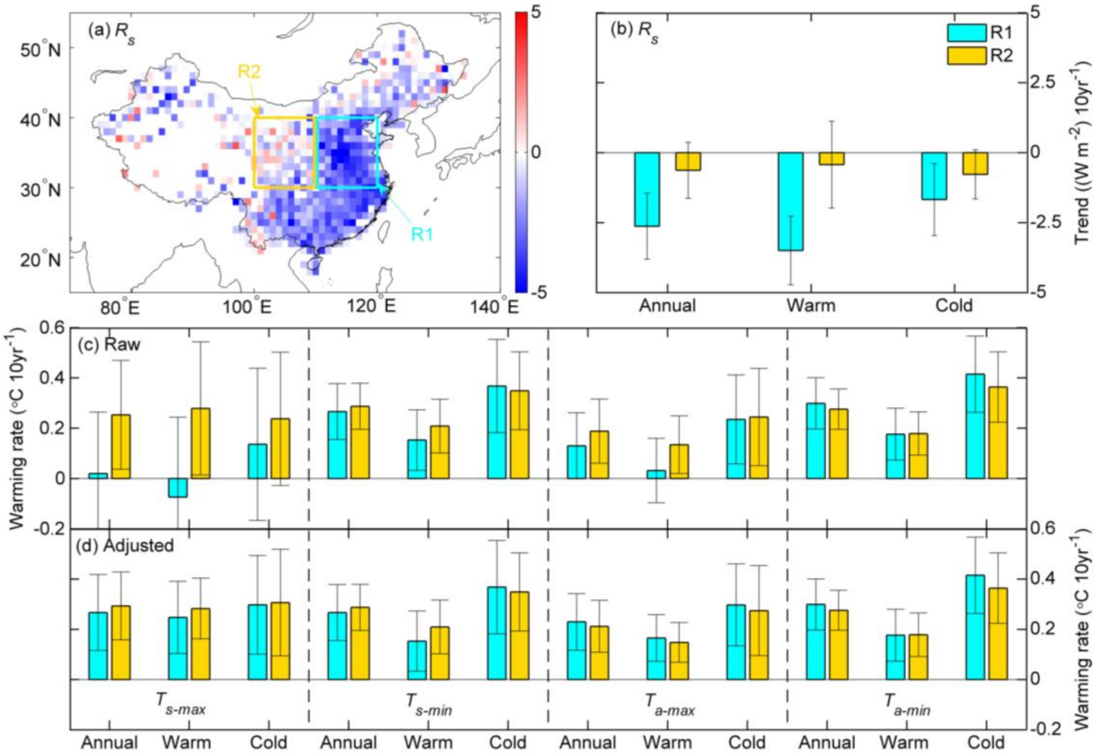

Figure 9. (a) Maps of the trends of surface solar radiation (R_s) and the location of the regions selected for further analysis: R1 (latitude: 30°-40° N; longitude: 110°-120° W) and R2 (latitude: 30°-40° N; longitude: 100°-110° W). (b) National mean trends for R1 and R2. (c) Annual, warm, and cold seasonal scale trends calculated based on the data before adjusting the effect of R_s and P. (d) Annual, warm, and cold seasonal scale trends calculated based on the data after adjusting the effect of R_s and P. All error bars indicate the 95% confidence interval.

Table 1. Warming rates (unit: °C $10yr^{-1}$) of the temperatures ($T_{s\text{-}max}$, $T_{s\text{-}min}$, $T_{a\text{-}max}$, $T_{a\text{-}min}$) for the annual, warm and cold seasonal scales. Raw and Adjusted represent the warming rates calculated for the data before and after adjusting for the effect of surface solar radiation (R_s) and precipitation (P), respectively. In Method I, the national mean anomalies were calculated first and then the national mean trend based on this time series was calculated. In Method II, the trend of each grid was calculated first and then the national mean value of the trends of all grids was calculated using the area-weight average method. We calculated the national mean trends of the temperatures using both methods.

			$T_{s\text{-}max}$	$T_{s\text{-}min}$	$T_{a\text{-}max}$	$T_{a\text{-}min}$
Method I	Raw	Annual	0.227±0.091	0.315±0.058	0.167±0.068	0.356±0.057
		Warm	0.172±0.103	0.221±0.054	0.091±0.056	0.245±0.049
		Cold	0.354±0.149	0.447±0.101	0.294±0.123	0.505±0.098
	Adjusted	Annual	0.373±0.068	-	0.222±0.062	-
		Warm	0.350±0.064	-	0.160±0.046	-
		Cold	0.450±0.119	-	0.329±0.114	-
Method II	Raw	Annual	0.254±0.197	0.328±0.094	0.183±0.103	0.368±0.082
		Warm	0.193±0.285	0.235±0.095	0.104±0.109	0.256±0.081
		Cold	0.321±0.267	0.415±0.159	0.264±0.167	0.476±0.139
	Adjusted	Annual	0.401±0.137	-	0.239±0.086	-
		Warm	0.374±0.173	-	0.174±0.082	-
		Cold	0.432±0.208	-	0.304±0.152	-

Units: °C $10yr^{-1}$. ±95% Confidence interval.